Taylor & Francis
Taylor & Francis Group

Particulate Science and Technology

An International Journal

ISSN: 0272-6351 (Print) 1548-0046 (Online) Journal homepage: https://www.tandfonline.com/loi/upst20

Circulating fluidized bed reactors – part 01: analyzing the effect of particle modelling parameters in computational particle fluid dynamic (CPFD) simulation with experimental validation

Janitha C. Bandara, Rajan Thapa, Henrik K. Nielsen, Britt M. E Moldestad & Marianne S. Eikeland

To cite this article: Janitha C. Bandara, Rajan Thapa, Henrik K. Nielsen, Britt M. E Moldestad & Marianne S. Eikeland (2019): Circulating fluidized bed reactors – part 01: analyzing the effect of particle modelling parameters in computational particle fluid dynamic (CPFD) simulation with experimental validation, Particulate Science and Technology, DOI: 10.1080/02726351.2019.1697773

To link to this article: https://doi.org/10.1080/02726351.2019.1697773

Published online: 15 Dec 2019.

PARTICULATE SCIENCE AND TECHNOLOGY
https://doi.org/10.1080/02726351.2019.1697773

Taylor & Francis
Taylor & Francis Group

Circulating fluidized bed reactors – part 01: analyzing the effect of particle modelling parameters in computational particle fluid dynamic (CPFD) simulation with experimental validation

Janitha C. Bandara[a], Rajan Thapa[a], Henrik K. Nielsen[b], Britt M. E Moldestad[a], and Marianne S. Eikeland[a]

[a]Department of Process, Energy and Environmental Technology, University of South-Eastern Norway, Porsgrunn, Norway; [b]Department of Engineering Sciences, University of Agder, Grimstad, Norway

ABSTRACT

A CPFD hydrodynamic model was developed for a circulating fluidized bed system and the simulation results were validated against experimental data based on particle circulation rate. Sensitivity of the computational mesh was primarily tested and extended grid refinement was needed at the loopseal to match the particle circulation rate with experimental data. The particle circulation rate was independent of the range of number of computational particles used in this study. A 10% reduction of the particle circulation rate was observed as the particle-wall interaction parameter was changed from 0.85 to 0.55 and 17% increment when the close-packed volume fraction was changed from 0.56 to 0.62. The pressure constant in the particle stress model showed the greatest impact for the circulation rate with 57% increment as the constant was changed from 2.5 to 5. The highest absolute variation in the pressure was observed at the loop seal and pressure values were under predicted in all sections.

HIGHLIGHTS

- CPFD simulations are efficient in analyzing fluidized bed systems.
- Manipulating of particle circulation rate is important in circulating fluidized bed.
- Pressure constant in particle stress model is the most influential factor.
- Uncertainties should be minimized prior to optimization of model parameters.

KEYWORDS

Circulating fluidized bed; particle circulation rate; CPFD simulation; sensitivity analysis; model parameters

1. Introduction

Circulating fluidized bed (CFB) is one of the favored technologies in power generation industries due to its distinct advantages of high heat and mass transfer rates, homogeneous reactor temperatures, extended gas-particle contact time, low pollutant emission and fuel flexibility (Li et al. 2004, 2014; Tricomi et al. 2017). Enhanced particle mixing in CFB prevents the generation of hot and cold spots, which is important in gasification and combustion processes as highly exothermic reactions are involved. CFB can be a single/double reactor system as illustrated in Figure 1 or multiple reactor system according to the process requirement. In a single reactor system, the reactor operates at fast fluidization regime in which the particles are carried away with the gas flow, separated with a cyclone and recycled back to the reactor across a proper gas sealing mechanism such as loop seal, L valve, J valve, seal pots, etc. CFB technology is a superior choice to exchange/circulate the same particle phase between different reactors having distinctive reactive environments. Continuous operation, runtime particle regeneration and controlled material handling some other highlights of CFB. However, efficient and safe design of CFB systems require accurate predictions of the gas-particle behavior in wide range of process conditions, where the rate of particle circulation is one of the most important parameters (Klenov, Noskov, and Parahin 2017).

Experimental studies of fluidized beds are expensive in time and cost. Observation of the interior dynamics of particles demands high-end technologies such as electrical capacitance tomography, particle image velocimetry, and laser Doppler anemometry, etc. Further, the system optimization with a single experimental rig is challenging such as optimization of geometrical shape and dimensions, particle size and feeding positions, etc. Computational fluid dynamic (CFD) modeling and simulation is a remarkable substitution to mitigate aforementioned drawbacks, which have become more realistic and efficient with increased computer power and advanced numerical algorithms (Li et al. 2014). Single-phase CFD simulations produce accurate results more precise than a sensor can capture. In contrast, CFD modeling

CONTACT Janitha C. Bandara janitha.bandara@usn.no, janithjc@gmail.com University of South-Eastern Norway, Kjølnes ring 56, P.O. Box 203 N3901, Porsgrunn, Norway

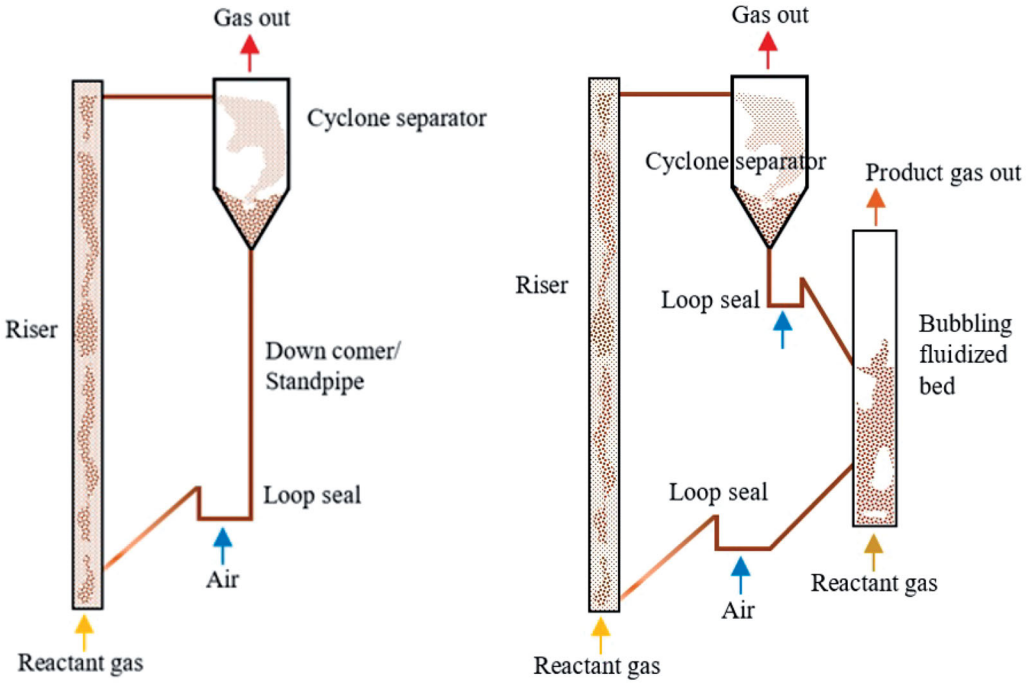

Figure 1. Different configurations of circulating fluidized bed. Circulating fluidized bed (left). Dual reactor circulating fluidized bed (right).

of multiphase flow systems are still challenging. Modeling of phase interactions and inter-particle collision with extended complexities aroused due to scale differences between particles of micron range and large reactors of several meters are the main challenges (Deen et al. 2007).

Eulerian-Eulerian (EE) and Eulerian-Lagrangian (EL) are the two fundamental approaches of multiphase CFD, which can be distinguished based on the treatment method of the dispersed phase. The fluid phase is modeled with Navier stokes equations with appropriate averaging method in both cases. Particle phase is mathematically treated as continuous and fully interpenetrating with fluid phase in EE modeling, while the trajectories of each particle are calculated in LE modeling. Kinetic theory of granular flow (KTGF) is used to derive the particle properties in EE method where the LE method uses Newton's second law of motion with hard-sphere or soft-sphere particle contact model. Empirical correlations are necessary at different levels for both EE and LE modeling (Deen et al. 2007). Even though the hydrodynamic predictions from EE simulations are recorded to be satisfactory by many researchers (Snider 2001; Chiesa et al. 2005), the discrete nature of the particles is missing (Chiesa et al. 2005; Jiang, Qiu, and Wang 2014). As the discrete particle method (DPM); LE method for particle systems, is concerned, approximately 80% of the computational cost is used to contact detections of particles and calculating the geometric areas of contact. Hence, increased number of particles in large-scale reactors imposes a substantial computational cost (Klenov, Noskov, and Parahin 2017) where DPM is not viable for industrial reactors in the near future. The computational efficiency of DPM is possible to boost by replacing the individual particle contacts with probabilistic strategy which is used in multiphase particle-in-cell (MP PIC) method (Pannala, Syamlal, and O'Brien 2011; Ma and Zhao 2018; Moliner et al. 2018).

The multiphase particle-in-cell (MP-PIC) method was developed by Andrews and O'Rourke (1996) and later by Snider (2001), to model dense particle flows. The actual particles are grouped into computational particles (parcels) that contain a number of adjacent particles sharing similar properties of density, size, and velocity. The parcel dynamics are modeled in the Lagrangian frame where the particle forces are calculated in the Eulerian grid considering the continuum approach. This reduces the extensive computational cost related to modeling of inter-particle collisions. Particle stress is calculated in an advanced time step, which is mapped back to individual particles in real-time with interpolation functions. Even with the superior computational efficiency, description of rotation movement and non-spherical shape of the particles are not included, which cause lower prediction accuracy compared to DPM. Detailed governing equations and numerical procedures of the MP PIC method can be found in the literature. (Andrews and O'Rourke 1996; Snider 2001; Snider and Banerjee 2010; Snider, Clark, and O'Rourke 2011; Chen et al. 2013; Jiang, Qiu, and Wang 2014).

Barracuda VR is a commercial CPFD package that is custom designed for particle systems using MP-PIC modeling. Tu and Wang (2018) have worked on a full loop CFB system to compare the energy minimization multi-scale (EMMS) and the Wen-Yu drag models with experimental validation. Jiang, Qiu, and Wang (2014) have carried out experiments in a six cyclone CFB and monitored the bed hydrodynamics using the electrical capacitance tomography (ECT) technique where the authors have carried out CPFD simulations for the same unit to compare the accuracy of the prediction. Chen et al. (2013) have used the CPFD technique to analyze the performance of a riser section of a CFB and commented on the requirement of drag model optimization. An extended validation of CPFD simulation has

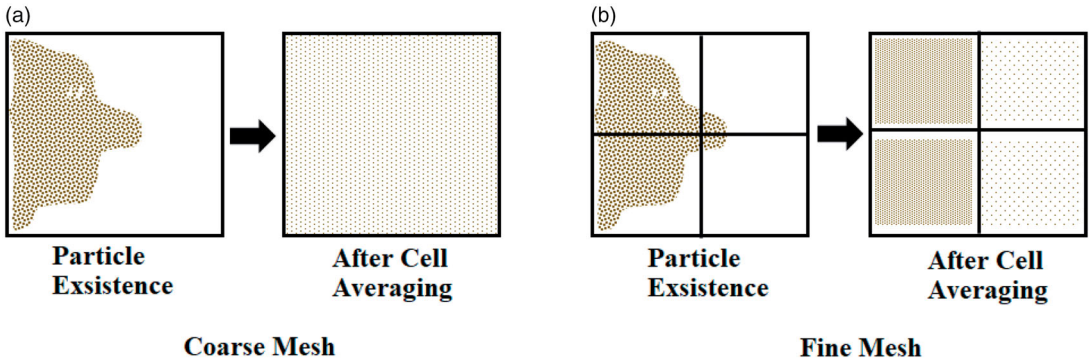

Figure 2. Effect of the mesh size in cell averaged particle volume fraction.

been done by Liang et al. (2014) with the experiments carried out in a bubbling fluidized bed and suggested some required improvements in the simulation setup. CPFD simulations have been used to analyze the nonreactive fluidized bed systems (Snider 2007; Qiu, Ye, and Wang 2015) and reactive systems like combustion and gasification of biomass and coal. (Snider and Banerjee 2010; Abbasi, Ege, and de Lasa 2011; Snider, Clark, and O'Rourke 2011; Xie et al. 2012; Loha, Chattopadhyay, and Chatterjee 2014; Thapa et al. 2016).

Multiphase flows exist in various forms of structures over a wide range of time and length scales (Li and Kwauk 2003). Computational mesh/grid should be sufficiently refined to capture these important mesoscale structures. The effect of the mesh size for cell averaged particle volume fractions is illustrated in Figure 2. Coarse grids destroy the small particle structures while the fine grids lead to high computational cost. In contrast to the DPM, selected particle properties are calculated based on the Eulerian grid in CPFD, which leads to definite effects from the grid size. Local small structures cause large variations in the particle volume fraction over the geometry, which impose a strong influence on interphase momentum and mass transfer by governing the drag force and mass transfer rate (Wang et al. 2010). Therefore, efficient capturing of these structures is crucial in accurate predictions in circulating fluidized bed operation.

The CPFD method further differs from DPM as it models computational particles instead of individual particles in the Lagrangian frame. Therefore, the resolution of the computational particles has an equal importance as the mesh resolution. However, with the implementation of "global cloud resolution" option, the number of computational particles in the system is adjusted accordingly with the cell size and number of cells in the initial particle patch.

Circulating fluidized bed configuration is a widespread technology in combustion and gasification of biomass. Biomass particles are difficult to fluidize due to their low density and irregularity in shape (Cui, and Grace 2007) and therefore, gasification reactors require a supporting particulate phase (bed material) consisting of fine fluidizable particles such as inert sand or catalysts. Despite the fact that the CFD simulation overcomes numerous practical limitations, extensive validation of hydrodynamic models is important for guaranteed data reproducibility. The reactor hydrodynamic is primarily governed by the bed material and hence, a detailed understanding of the hydrodynamics of bed material in a non-reactive CFB system is important for subsequent CFD analysis in a reactive environment. A similar CFB geometry has been analyzed and presented by Wang et al. using CPFD in two consecutive research articles (Wang et al. 2014a, 2014b). Nevertheless, the effects of the coefficients in particle stress model and particle-wall contact momentum retention are not presented. The particle flow across the loop seal happens in dense phase and as a result, the particle weight is directly applied on the bottom and sidewalls of the loop seal. The pipe cross-section at the loop seal is narrow and therefore, it is expected that the wall friction exert a significant effect over a considerable fraction of the cross-section available for the particle flow. Even though specific values have been defined for hard and soft particles in the technical guidance of Barracuda VR, a sharp shift between soft and hard particles is not real. Hence, the effects of the particle-wall collision parameters are presented, which will be useful for those who need extended tuning. Unlike in bubbling fluidized beds, there exists a resultant particle flow driven by fluid drag and particle collisions against gravity and contact forces (particle-particle and particle-wall). Further, unlike in dilute phase particle flow, the dense phase particle flow across the loop seal is greatly affected by the inter-particle forces. Particle stress model is responsible for calculating the particle-particle forces, which is significant as it reaches the close packing. Therefore, the effects of particle-wall collision and particle stress model parameters are analyzed and presented along with a comprehensive analysis of the effects of grid size, number of computational particles, close pack volume fraction and fluid drag model. The simulation results are compared with experimentally measured rate of particle circulation and system pressure. Barracuda VR 17.3.0 CPFD commercial software was used in this work with Intel(R) Core(TM) i7-5930K CPU 3.50 GHz processor.

2. Experimental and CFD model set up

Model validation is based on experimental studies performed in a full loop CFB unit, which is illustrated in Figure 3. Detailed experimental procedure is given in the work of Thapa et al. (2016). Sand with particle density of 2650 kg/m^3 and mean diameter of 150 µm was used as the particle phase and air was used as the fluidizing medium.

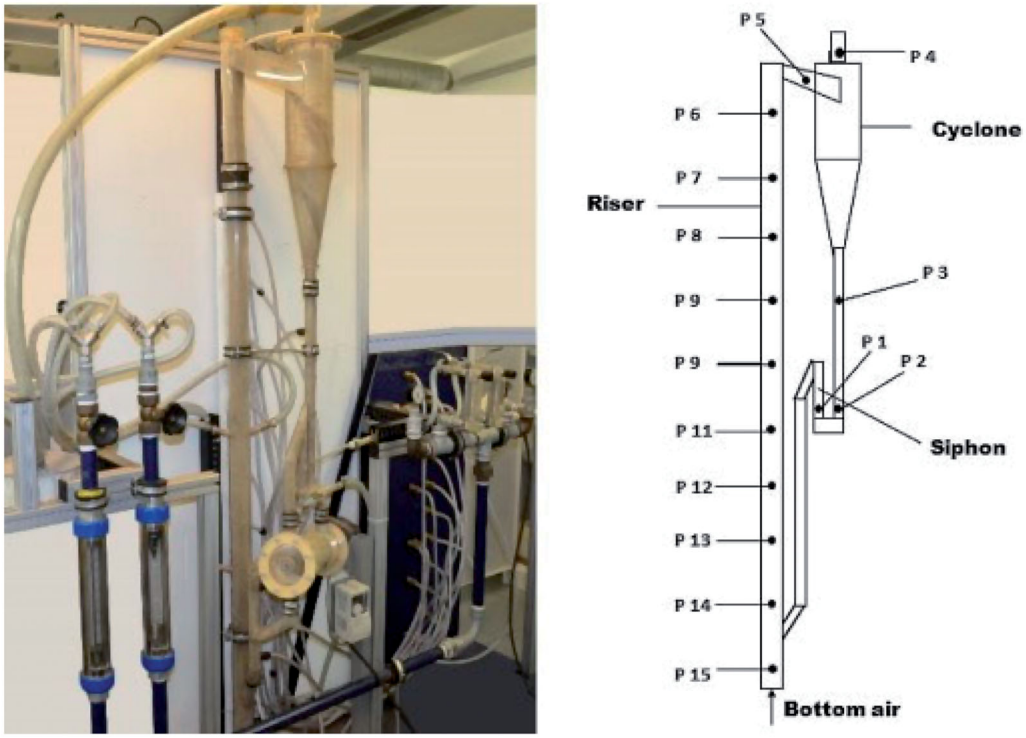

Figure 3. Circulating fluidized bed experimental rig.

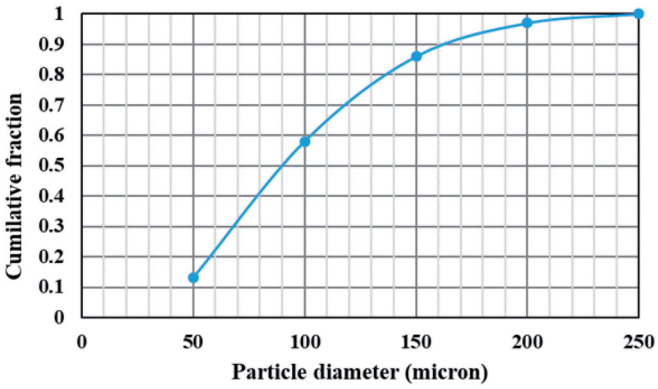

Figure 4. Particle size distribution of the bed material.

The particle size distribution was ranged from 50 to 250 µm and illustrated in Figure 4. The geometrical dimensions were adopted from a scaled drawing. The diameter of the standpipe and the recycle pipe are 30 mm. The horizontal section of the loop seal is 70 mm long and has a cross-section area of 30 mm × 30 mm. The height of the recycle pipe before the sharp bend is 135 mm. The riser section is 50 mm in diameter and 1700 mm in height. The technical terms related to loopseal sections are defined by Basu and Butler (2009).

A summary of the boundary values, particle properties, and modeling parameters are given in Table 1. The boundary conditions, computational mesh, and initial particle filling are depicted in Figure 5. The fluidizing air to the riser was implemented as a uniform flow boundary throughout the bottom plane of the column and loopseal aeration with

Table 1. Simulation data and model parameters.

Particle mean diameter	130 micron
Aeration gas	Air
Riser fluidized air	20 Nm^3/h
Loop seal aeration	1 Nm^3/h
Particle mass	0.58–0.6 kg
Close pack volume fraction	0.6
Collisional momentum redirection	40%
Normal-to-wall momentum retention	0.85
Tangent-to-wall momentum retention	0.85
Initial time step	0.0005 s

injection boundaries as illustrated in Figure 5(b). The initial particle patching was implemented as illustrated in Figure 5(c) and pressure-monitoring points were implemented at P1, P2, P3, P6, and P15 as illustrated in Figure 3. Two flux planes along the standpipe and the recycle pipe were positioned to monitor the particle circulation rate.

Particle stress model was used with default parameters of 1, 3, and 10^{-8} for P_s, β, and ε, respectively. The "blended acceleration model" (BAM) was activated, as the particle phase had a size distribution in the range of 50–250 microns. BAM prevents unrealistic particle segregation by absorbing the sustained particle contacts that is prevalent in dense particle systems. A considerable effect was expected related to particle-wall interaction and hence, the diffuse bounce coefficient (a measure of deviated angle from ideal after collision) was set to 3. Turbulence was modeled with large eddy simulation and the numerical scheme used was Partial Donor Cell (PDC) method, which is a weighted average formulation of central difference and upwind schemes. Courant-Friedrichs-Lewy (CFL) condition is a measurement of the stability of the numerical solver whereas of 0.8 and

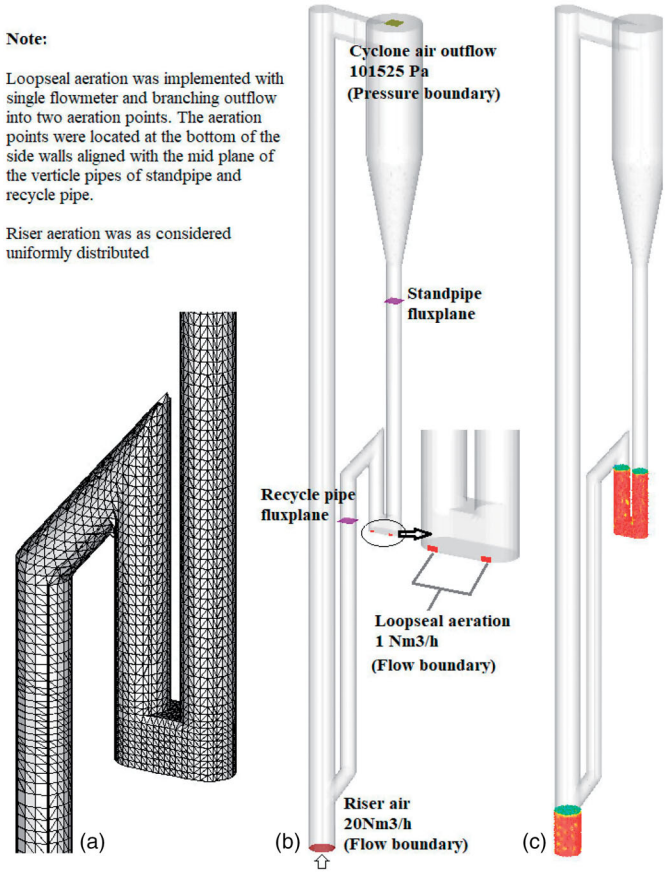

Figure 5. (a)-Computational grid near loopseal, (b)-Boundary conditions and Flux planes, (c)-Initial particle filling.

1.5 were used for minimum and maximum values, respectively. The grid sensitivity analysis was carried out using Wen-Yu-Ergun drag model. The particle-wall interaction coefficients were taken as 0.85 for both normal and tangential collisions as specified by Barracuda VR for hard particles. The closed-pack volume fraction was set as 0.6. The grid convergence (grid sensitivity analysis) test and the effect of computational particles were performed to identify the optimal grid having less computational time with sufficient accuracy. The hydrodynamic model with optimized grid and computational particles was subsequently analyzed for different particle-wall interaction coefficients for perpendicular collisions. The model was subjected to further analysis to identify the effect of the closed-pack volume fraction of particles, pressure constant of particle stress model and four different fluid drag models.

2.1. Governing equations

The drag model is one of the crucial parameters that governs the particle behavior. The riser operates in the dilute phase while the standpipe of the loop seal (dip leg from the cyclone) is supposed to operate in dense phase at either minimum fluidization or packed bed. The Ergun equation has been extensively analyzed and proved for its high accuracy in the dense particle phase and therefore, the Gidaspow drag model, which is a blended formulation of the Wen-Yu and Ergun drag models, was used for the initial simulation works. The Wen-Yu drag model is used at gas volume fractions higher than 0.8 (Patel, Pericleous, and Cross 1993; Jayarathna et al. 2019).

$$D_{Wen-Yu} = \frac{3}{8}\ C_d\ \frac{\rho_g}{\rho_p}\ \frac{|u_g - u_p|}{r_p}\ \alpha^{-2.65}$$

$$C_d = \frac{24}{Re},\ (Re < 0.5)$$

$$C_d = \frac{24}{Re}(1 + 0.115Re^{0.687}),\ (0.5 \le Re \le 1000)$$

$$C_d = 0.4,\ (Re > 1000)$$

C_d is the drag coefficient, Re is the particle Reynolds number and r_p is the particle diameter. As the gas volume fraction decreases below 0.8, the Ergun correlation is used (Ergun 1952; Jayarathna et al. 2019),

$$D_{Ergun} = 0.5\left(\frac{C_1\alpha_p}{\alpha_g Re} + C_2\right)\frac{\rho_g}{\rho_p}\ \frac{|u_g - u_p|}{r_p}$$

The default values for the laminar and turbulent coefficients in the Barracuda VR are 180 (C_1) and 2.0 (C_2) where those are 150 and 1.75 in original Ergun formulation. The particle Reynolds number is given by:

$$Re = \frac{2\rho_p|u_g - u_p|}{\mu_g}\left(\frac{3V_p}{4\pi}\right)^{1/3}$$

The gas phase mass and momentum conservation are modeled with continuity and time-averaged Naiver-Stokes equations (Snider 2001):

$$\frac{\partial(\alpha_g\rho_g)}{\partial t} + \nabla \times (\alpha_g\rho_g u_g) = 0$$

$$\frac{\partial(\alpha_g\rho_g u_g)}{\partial t} + \nabla \times (\alpha_g\rho_g u_g u_g) = -\nabla P - F + \nabla \times (\alpha_g\tau_g) + \alpha_g\rho_g g$$

Where α_g, ρ_g, and u_g are gas phase volume fraction, density, and velocity, respectively. F is the total momentum exchange with particle phase per volume, g is the gravitational acceleration, P is the pressure, and τ_g is the gas phase stress tensor. The stress tensor the gas phase is given by,

$$\tau_g = \mu_g\left[\left(\nabla u_g + \Delta u_g^T\right) - \frac{2}{3}\nabla \times u_g I\right]$$

μ_g refers to the shear viscosity that is the sum of the laminar and turbulent components. The large eddy simulation is used for the large-scale turbulence modeling while the subgrid scale turbulence is captured with the Smagorinsky model:

$$\mu_{g,t} = C_s\rho_g\Delta^2\left|\nabla u_g + \Delta u_g^T\right|$$

Table 2. Properties related to different grid configurations.

Grid	Cells	Cell size (Δx, Δy, Δz) (mm)	Computational particles	Computational particles to cell ratio
01	136,000	7.5 × 7.5 × 7.5	5×10^4	0.367
02	242,592	6 × 6 × 6	9.2×10^4	0.379
03	338,541	5 × 5 × 5	1.33×10^5	0.392
Refined grids at loop seal (*the grid sizes at the loop seal)				
04	323,830	3.75 × 3.75 × 3.75*	1.86×10^5	0.574
05	401856	3.75 × 3.75 × 3.33*	2.35×10^5	0.584

The default value for the model constant C_s is 0.01. Δ is the sub-grid length scale and calculated by,

$$\Delta = (\delta x \delta y \delta z)^{1/3}$$

The interface momentum transfer is calculated through the viscous drag force:

$$F = \int\int f \left\{ m_p \left[D_p(u_g - u_p) - \frac{\nabla P}{\rho_p} \right] \right\} dm_p du_p$$

Subscript P refers to the particle phase properties where m and u symbolizes the mass and velocity, respectively. D_p is the drag function. The particle phase dynamics are derived using the particle distribution function (PDF) calculated from the Liouville equation given as (Snider 2001):

$$\frac{\partial f}{\partial t} + \nabla(f u_p) + \nabla u_p (f A_p) = 0$$

Where A_p is the particle acceleration and is expressed by:

$$A_p = \frac{\partial(u_p)}{\partial t} = D_p(u_g - u_p) - \frac{\nabla P}{\rho_p} - \frac{\nabla \tau_p}{\rho_p \alpha_p} + g$$

α_p is the particle volume fraction. τ_p is the particle stress function, which is used to formulate the interphase interactions of particles (Snider 2001; O'Rourke and Snider 2014).

$$\alpha_p = \int\int f \frac{m_p}{\rho_p} dm_p du_p$$

$$\tau_p = \frac{10 P_s \alpha_p^{\beta}}{max\left[(\alpha_{cp} - \alpha_p), \varepsilon(1 - \alpha_p)\right]}$$

P_s is a constant with the units of pressure, α_{cp} is the particle volume fraction at close packing, β is a constant between 2 and 5. ε is a very small number in the order of 10^{-7}, which is used to avoid the singularity as particles reach closed pack volume.

Turton–Levenspiel drag model (Turton and Levenspiel 1986):

$$D = \frac{3}{8} C_d \frac{\rho_g}{\rho_p} \frac{|u_g - u_p|}{r_p}$$

$$C_d = \frac{24}{Re} \alpha_p^{-2.65} \left[(1 + 0.173 Re^{0.657}) + \frac{0.413}{1 + 16300 Re^{0.657}} \right]$$

Nonspherical Ganser drag model (Chhabra, Agarwal, and Sinha 1999) where ω is the particle sphericity:

$$C_d = \alpha_p^{-2.65} K_2 \left[\frac{24}{Re\ K_1 K_2} \left(1 + c_0 (Re K_1 K_2)^{n_1}\right) + \frac{24 c_1}{1 + \frac{c_2}{Re K_1 K_2}} \right]$$

$$c_0 = 0.1118,\ c_1 = 0.01794,\ c_2 = 3305,\ n_1 = 0.6567,\ n_2 = 1.8148,\ n_3 = 0.5743$$

$$K_1 = \frac{3}{1 + 2\omega^{-0.5}},\ K_2 = 10^{n_2(-\log\omega)^{n_3}}$$

Nonspherical-Haider-Levenspiel drag model (Chhabra, Agarwal, and Sinha 1999):

$$C_d = \alpha_p^{-2.65} \left[\frac{24}{Re} \left[1 + c_0\ \exp(n_1 \omega)(Re)^{(n_2 + n_3 \omega)} \right] + \frac{24 c_1 \exp(n_4 \omega) Re}{Re + c_2 \exp(n_5 \omega)} \right]$$

$$c_0 = 8.1716,\ c_1 = 3.0704,\ c_2 = 5.378,\ n_1 = 4.0655,\ n_2 = 0.0964,\ n_3 = 0.5565,\ n_4 = -5.0748,\ n_5 = 6.2122$$

Richardson-Davidson-Harrison drag model follows the Wen-Yu drag model excluding the functionality of the effect of particle volume fraction.

3. Results and discussion

The particle circulation rate had been experimentally calculated by interrupting the loopseal aeration and measuring the time to build up a certain amount of particles (the bed height) in the standpipe (Thapa et al. 2016). This might substantially influence the particle hydrodynamics in the riser, as the particles are not fed to the riser from the loopseal. A precise measurement of the particle height in the standpipe is challenging during fluidization conditions. The particle circulation rate is highly fluctuating and local measurements might not represent the long-standing average of the system. Further, the system needed to be operated for a certain time to achieve the steady-state conditions prior to taking the measurements where a slight fraction of the particle mass can be escaped. Hence, there can be a discrepancy in system mass between experiments and simulations.

Moreover, uncertainties related to the CPFD model set up might lead to deviations from the actual settings. CPFD requires to feed the envelope density[1] and however, the apparent density of 2650 kg/m^3 was used due to insufficient data of particles. Assumption of spherical particles and uncertainty of the particle size distribution might lead to

[1]Absolute density is excluding volume of open and close pores of the grain (absolute volume of the particle material) while apparent density is excluding only close pores. Envelope density is calculated by taking average shape of the particle (i.e. including narrow open pores) whereas, inter particle voids are also included in bulk density measurements.

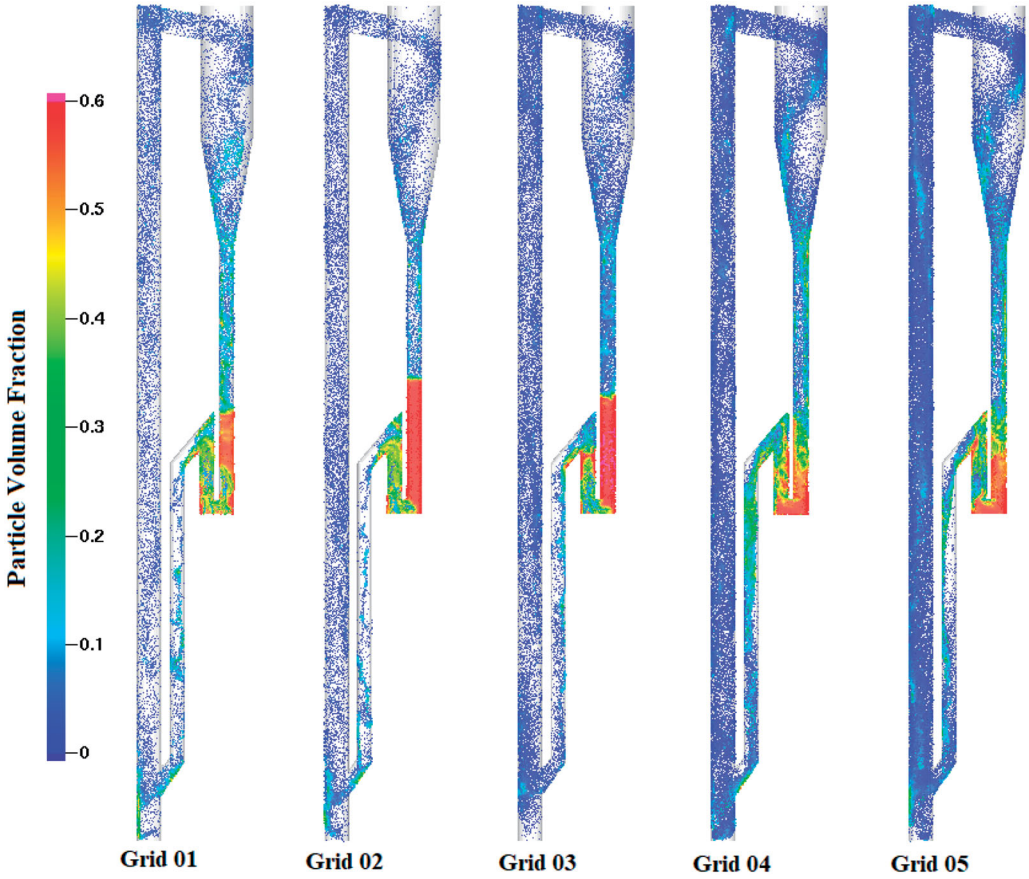

Figure 6. Particle volume fractions at 30th second of the simulation for different grid configurations.

deviations in hydrodynamics of fluidization followed by particle circulation rate.

3.1. Grid sensitivity

The solid circulation rate and the system pressure were analyzed with five different grid configurations. Grid 01, 02, and 03 were constructed using uniform grid option. Grids 04 and 05 were constructed by refining the cell structure simply at the loopseal of Grid 01 and 02, respectively. Table 2 summarizes the number of cells, grid size, and number of computational particles of each grid configuration.

As the number of computational cells is increased, a simultaneous increment of computational particles can be observed. The graphical representation in Figure 6 illustrates the computational particles (i.e. not the real particles). A gradual increment of computational particles towards fine mesh grids is clearly visible from Grid 01 to 05. The ratio between the computational particles to the number of cells is nearly equal in Grid 01, 02, and 03 while Grid 04 and 05 show considerably higher values. As the number of cells is high at the loopseal in Grid 04 and 05, more computational particles are included by the model setup.

Particles tend to accumulate along the standpipe in the coarse grids 02 and 03. Bubbles cannot be observed and hence, the particle bed is either at the packed bed regime or at minimum fluidization conditions. This results in less particle concentration in the other sections of the system, especially in riser. In contrast, Grid 04 and 05 show rigorous fluidization at the loopseal. The gas jet penetration length at the loopseal aeration was also observed. In the coarse grid simulations, the gas jet dissolves near the injection and does not move much in the direction of the injection. In contrast, the penetration length is high in the refined girds, which might lead to different hydrodynamics at the loopseal and consequently affect the particle circulation rate. Whenever the grid structure changes, the number of parcels, parcel size, and consequently, the number of parcels per cell are changed.

3.1.1. Particle circulation rate

The particle circulation rate is analyzed across the flux plain defined at the recycle pipe (Figure 5). The averaged values over 30th second for different grid configurations and the experimental value are illustrated in the right upper chart of Figure 7. The circulation rates, averaged over two-second intervals of the simulation, are depicted in the right middle plot of Figure 7. Grid 01 shows extremely low circulation rate of 30 kg/h and the grid resolution is insufficient to capture the particle hydrodynamics. A significant improvement of the particle circulation up to 220 kg/h was achieved by a uniform grid refinement towards Grid 02 and 03. However, a substantial difference between Grid 02 and 03 could not be observed even with 100,000 more cells in Grid 03 than in Grid 02. With the observed particle accumulation at the standpipe, successive grid refinements at the loopseal were performed for detailed analysis. Grid 04 and 05 are the

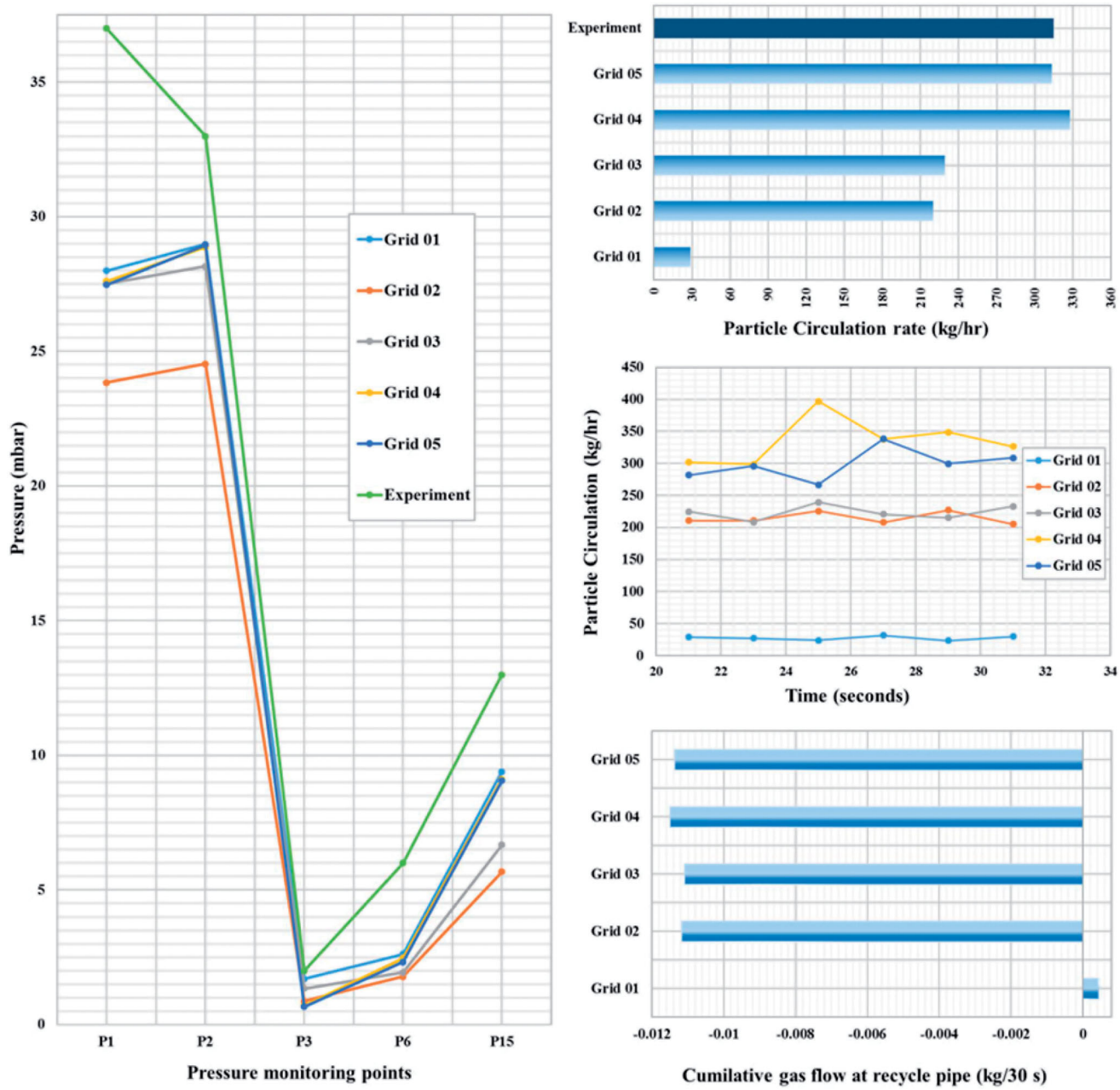

Figure 7. Particle circulation rate and pressure profiles for different grid configurations.

restructured meshes at the loopseal of Grid 02 and 03, respectively. A sensible improvement can be observed in both of the grids 04 and 05 having average circulation rates of 325 kg/h and 315 kg/h, respectively, which is approximately equal to the experimental results. Apart from the extreme deviation at the 25th second, Grid 04 and 05 follow a similar behavior and finally reach a near steady value around 320 kg/h. The circulation rate at the recycle pipe was compared with the additional flux plane defined at the standpipe to verify the steady-state operation. A slight difference between the two flux planes was observed in Grid 01 and 02 whereas Grid 03, 04, and 05 had equal values.

The instant variations of the solid circulation rates between Grid 04 and 05 can be due to different grid structures in the riser, loopseal and cyclone followed by a different number of computational particles at each setup. Large variations in the cell sizes over the domain are not recommended and further, the lengths in X, Y, and Z directions of a certain cell should be uniform if possible. Further, a sharp change in the cell size should be prevented by implementing a gradient in the direction of change. The number of computational particles is defined based on initial particle patching and the cell sizes in the patching volume. The number and volume of computational particles remain constant in time (for a closed loop system). Whenever computational particles of different sizes exist in the system, the largest should be fine enough to enclose in the finest cells in the domain. The difference in the cell sizes between the loop seal and the rest of the domain is higher in Grid 04 compared to Grid 05. Especially, the meshing near the walls of the cyclone cylindrical section is relatively coarse in Grid 04. This might lead to a slight excess

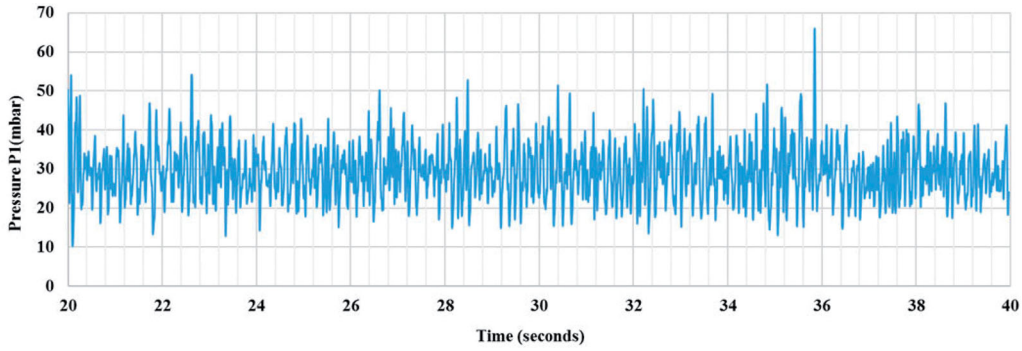

Figure 8. Instantaneous pressure values at P1 from simulation of Grid 04.

prediction of particle circulation when using Grid 04. Grid 05 delivers exactly the same particle circulation rate as that in experiments.

The loopseal aeration had been achieved by two injection points and however, measured by a single flowmeter (during experiments). A slight difference in the pressure at two particular locations could be observed and hence, the related flowrates could be different from each other. Implementing narrow injection pipes in the computational setup requires very fine meshing at the loopseal. Therefore, each aeration point was implemented using injection boundary conditions (in contrast to the standard flow boundaries) with half of the total measured loopseal airflow. The CFB setup has narrow pipes and passages and therefore, minor errors/uncertainties related to lengths might lead to considerable deviations in the simulations results. Due to these uncertainties and simplified implementations in the CPFD setup, the hydrodynamic behavior in the simulations can deviate from the experimental results.

The gas flow behavior across the recycle pipe was also monitored at the same flux plane used to monitor the particle circulation. The results are illustrated to the right at the bottom of Figure 7. The cumulative gas flow after 30 seconds of simulation was compared between the different grids. According to the proper functionality, gas is not expected to pass from the riser through the loopseal to the cyclone. Instead, part of the loopseal-air flows towards the riser, which gives a negative flux in Z direction. Grid 01 displays a positive flux, which is not the expected flow behavior. The rest of the grid tests show an approximately equal negative flow of 0.0115 kg during 30 seconds. The calculated cumulative airflow at the loop seal from the injection boundary conditions is 0.01122 kg, which is nearly equal to 0.0115 kg. However, a slightly higher airflow can be observed in Grid 04 and 05 compared to Grid 02 and 03. The particle circulation is substantially high for these grids and therefore, an additional amount of gas is carried along with the particles. The particle flow in the loopseal is mainly driven by the gas drag and not by the pressure exerted by the standpipe particle inventory.

3.1.2. System pressure

The system pressure at selected locations is plotted in Figure 7 and the simulation results represent the averaged values between 25 and 30 seconds. The numbering of pressure locations is referred to Figure 3. Grid 2 shows the highest deviation of the pressure compared to the experimental results whereas P_1 shows the highest local variation when all the grid configurations are considered. The pressure data obtained from the simulations follows the same trend as experimental values except for P_1. P_1 is higher than P_2 during the experiments, whereas P_1 is lower than P_2 in all the simulations. This deviation might be related to the uncertainty of the geometrical dimensions; especially the height of the recycle pipe and pipe diameter of the loopseal. The instantaneous pressures values at P_1 for Grid 04 are illustrated in Figure 8 and high fluctuations between 15 and 45 mbar can be observed. The simulation results reach the experimental value at certain times and therefore, it is recommended to average the pressure data over an extended time (in experiments and simulations).

Assumption of spherical particles, uncertainty related to particle size distribution and implemented closed packed volume fraction followed by deviations in the particle inventory and geometrical dimensions can be the root cause for the pressure deviation between simulation results and experimental data. Further, the particle volume fraction of the riser varies between 0 and 0.1 (Figure 6). The Wen-Yu correlation is used to calculate the fluid drag force at lower particle volume fractions according to the model definition. The drag model for dilute phase flows has not been extensively validated as for the dense phase systems such as packed beds or bubbling fluidized beds. Hence, the low pressures in the riser can be due to reduced particle loading where this particular variation effects on the other sections as well. On the other hand, the Ergun correlation has been developed using Geldart B particles. However, the used particle mixture was at the margin of the Geldart A and B particles, where a fraction of the mixture is classified as Geldart A particles. Therefore, the linear coefficient of the laminar component of the Ergun correlation can be deviated from the original value of 150, which can exert a considerable effect on the pressure profile, especially at the loopseal.

3.2. Effect of the number of computational particles

Even with the analogous pressure profiles, Grid 01 results in reduced particle circulation with unrealistic gas flow behavior and therefore, further analysis was discarded. A

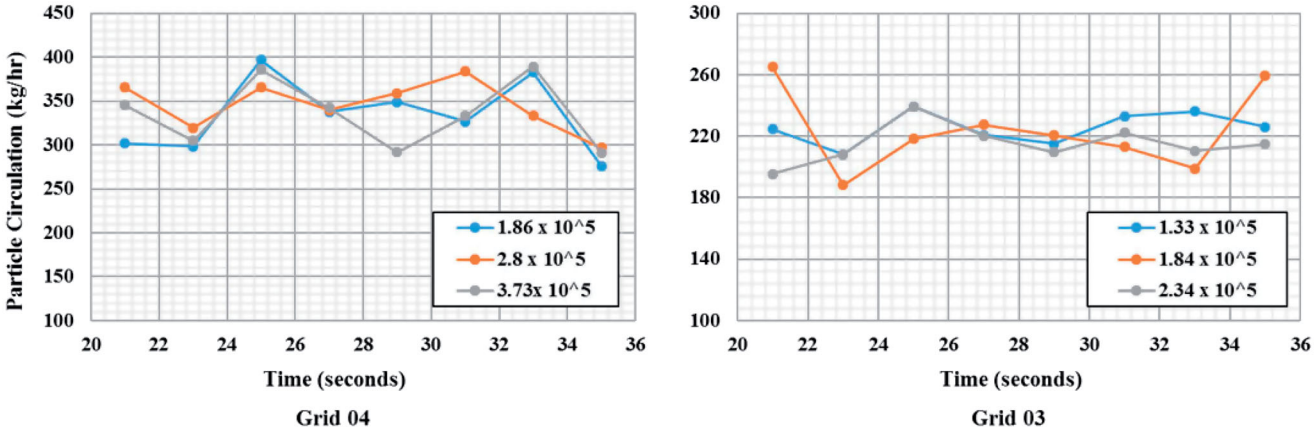

Figure 9. Particle circulation rate with increased computational particle.

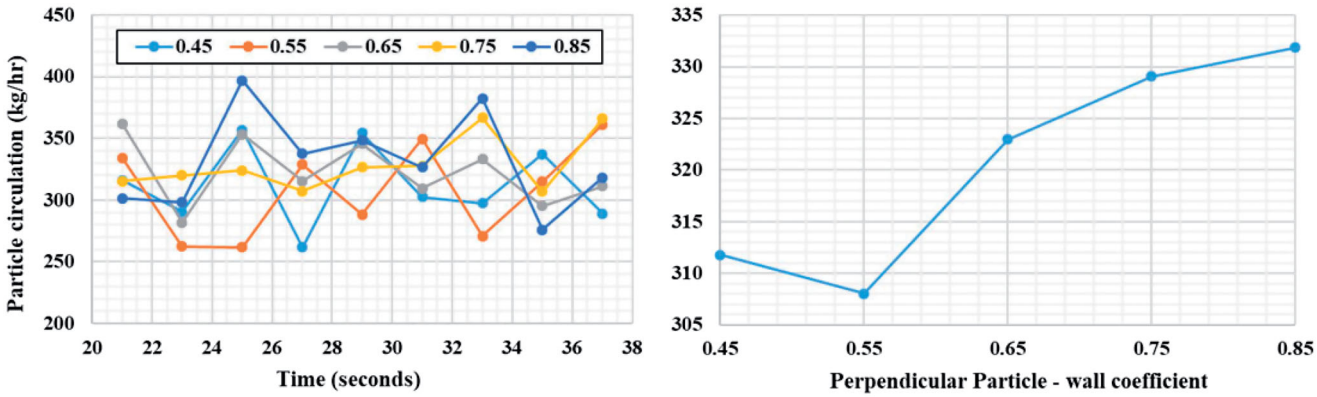

Figure 10. Sensitivity of particle-wall interaction for particle circulation rate.

substantial growth in the particle circulation (approximately 40%) was observed when the grid was refined from Grid 03 to 04. The number of computational particles is a function of the grid that encloses the initial particle patching and it remains unchanged during the simulation unless the system mass is changed. The successive grid refinements from 01 to 05 caused increasing number of computational particles and therefore, supplementary analyses were necessary to verify whether the increased circulation was achieved due to the grid refinement or the increased number of computational particles. Two additional simulations were performed for Grid 03 with 1.84×10^5 and 2.34×10^5 computational particles, which are the same number of particles used in the original Grid 04 and 05, respectively (Table 2). Computational particle convergence analysis was carried out for Grid 04 with two subsequent simulations having 2.8×10^5 and 3.73×10^5 particles.

The simulation results are depicted in Figure 9 and there was not observed any considerable change in the average particle circulation with increased number of computational particles. However, local differences of the circulation rates can be observed for both grids. Therefore, it can be concluded that the bed hydrodynamics has not been affected by changing the number of computational particles. Further, the pressure profiles follow similar characteristics irrespective of the computational particles. Therefore, Grid 04 with 1.86×10^5 computational particles was used for further analysis.

3.3. Effect of the particle-wall interaction coefficient

The particle-wall interaction is modeled with three parameters of perpendicular collision, tangential collision, and diffuse bounce. The default recommended values for the perpendicular and tangential collision are 0.3 and 0.99, which have been used by many researchers. The effect of these parameters are minimal for vertical fluidized beds. The pipe diameter at the loopseal is narrow and the horizontal passage operates at dense phase where the particle weight directly applies on the pipe walls. Hence, loopseal operation can be considerably affected by particle wall interactions and consequently, the particle circulation rate. Hard particles can be modeled using 0.85 for both coefficients as recommended by Barracuda VR. The perpendicular coefficient was changed from 0.45 to 0.85 (keeping tangential coefficient constant at 0.85) and the particle circulation rate was monitored. The diffuse bounce was set to 3 for all simulations, which carries the information of scattering angle related to particle-wall collisions.

The plots in Figure 10 reflects the instantaneous and 30 second averaged particle circulation rates. The circulation

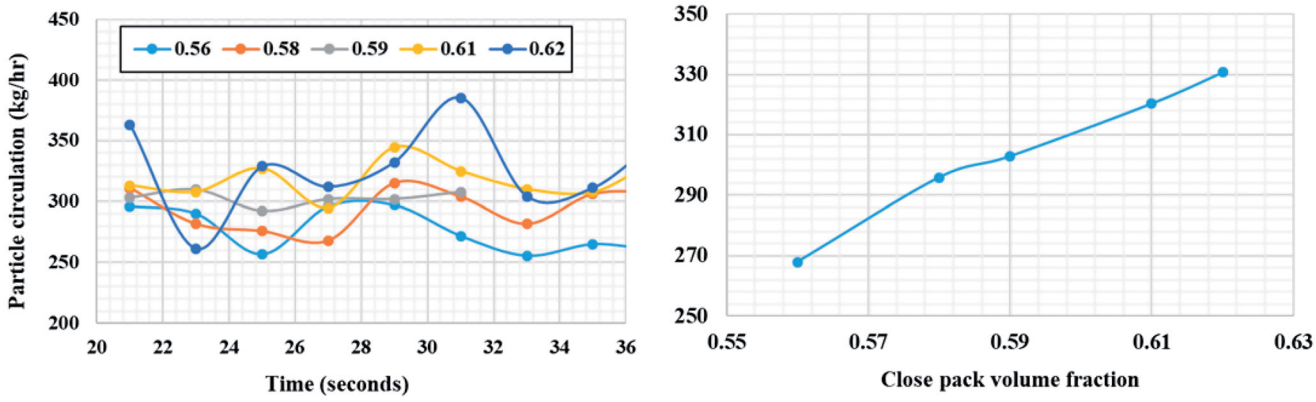

Figure 11. Particle circulation as a function of closed pack volume fraction.

rate increases proportionally with the particle-wall interaction coefficient in the range of 0.55–0.85. The circulation rate is more sensitive to the coefficient at low values and becoming less sensitive at higher values.

3.4. Effect of the closed pack volume fraction

Closed pack volume fraction carries the information about the degree of maximum packing. The higher the value, the more the resistance for the fluid to penetrate through and hence, the pressure drop is increased. In contrast, the fluid drag correlation is a function of particle volume fraction. Further, the particle stress model uses the closed pack volume fraction in calculating the force exerted from particle collisions. These factors influence the particle hydrodynamics and hence, the closed pack volume fraction is one of the most important parameters in MP PIC modeling. The close pack volume fraction is simply calculated by bulk density to particle density ratio and however, only particle size distribution and absolute density were available. Therefore, the particle circulation rates for different values of closed pack volume fraction were analyzed and the results are given in Figure 11.

A proportional increment in circulation rate can be observed. Referring to the time dependent rate, higher fluctuations can be observed as the closed pack volume fraction is increased and however, the fluctuations are minimum at 0.59. The loopseal pressure readings slightly increased with high close pack volume fractions. As the close pack volume fraction is involved in both drag model and stress model, the observed effect of increasing circulation has two roots. Therefore, extended simulations were conducted changing the pressure constant in stress model equation.

3.5. Effect of pressure constant in particle stress model

The modeling of particle-particle interactions is crucial in dense particle systems, which requires a strong four-way coupling. The loopseal section is at dense phase in standard operating conditions and hence, the particle stress model can have a greater impact on hydrodynamics. As the particles reach close pack volume fraction, the denominator of the stress function reduces to a low number and consequently, the stress is increased generating high forces. The pressure constant itself contribute to increase the particle stress. As the loopseal operates at dense phase flow regime, this increased force can improve the circulation.

As mentioned in the section "Experimental and CFD model set up", loopseal aeration was implemented as injection boundary conditions where the mass flowrate and the injection velocity should be defined. The injection velocity showed a considerable impact on particle circulation rate and it was adjusted during grid sensitivity analysis. The optimized value was used for the following simulations in sections of "Effect of the particle-wall interaction coefficient" and "Effect of the closed pack volume fraction". However, as the pressure constant was changed from 1 to 5, the particle circulation rate increased unrealistically. As the main uncertainty appeared in loopseal aeration, the injection boundary was changed into flow boundary having an identical value to the inner area of 6 mm pneumatic pipe connection. The pressure constant was needed to increase beyond 4.5 to fix the circulation rate with experimental data as depicted in Figure 12. The pressure constant vs. particle circulation curve becomes flat between 3.5 and 4.5, however, the circulation increases proportionally with the pressure constant. The system pressure remained nearly similar irrespective of the different pressure constant values.

3.6. Effect of the fluid drag correlation

The Wen-Yu-Ergun drag model was used for all the prior simulations. The main drive to select this particular model was due to the existence of both dilute and dense phase in the system. Several inbuilt drag functions are available in Barracuda VR, where few models are equipped to model non-spherical particles. The Turton-Levenspiel, Nonspherical-Ganser, Nonspherical-Haider-Levenspiel, and Richardson-Davidson-Harrison drag models were compared with the Wen-Yu-Ergun model based on particle circulation rate. An additional simulation using the Wen-Yu-Ergun model with modified laminar and turbulent coefficients of 180 and 2, respectively (Barracuda default values), were carried out. The results are presented in Figure 13. The Richardson-Davidson-Harrison model showed extremely low circulation of nearly 150 kg/hr where more particles accumulated in the standpipe section of the loop seal. The

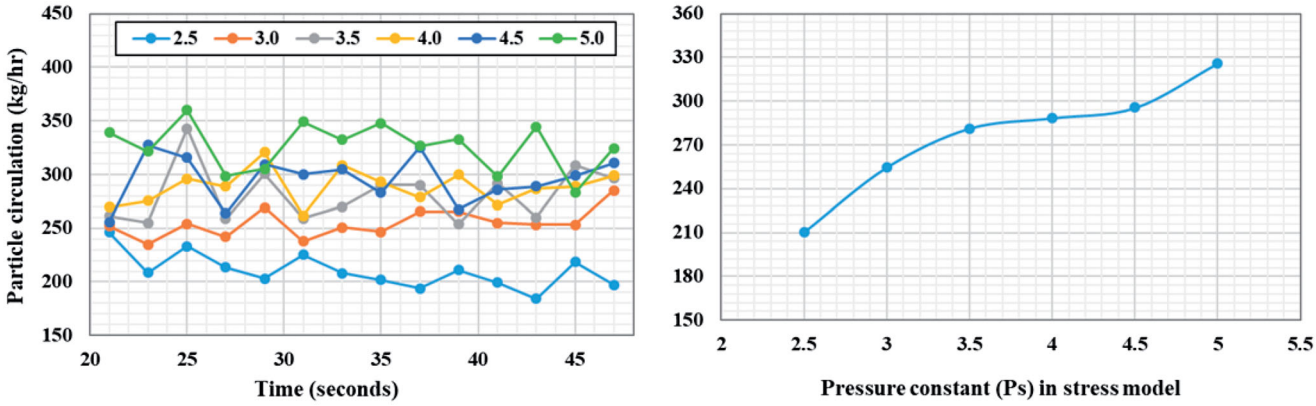

Figure 12. Effect of the pressure constant in the particle stress model.

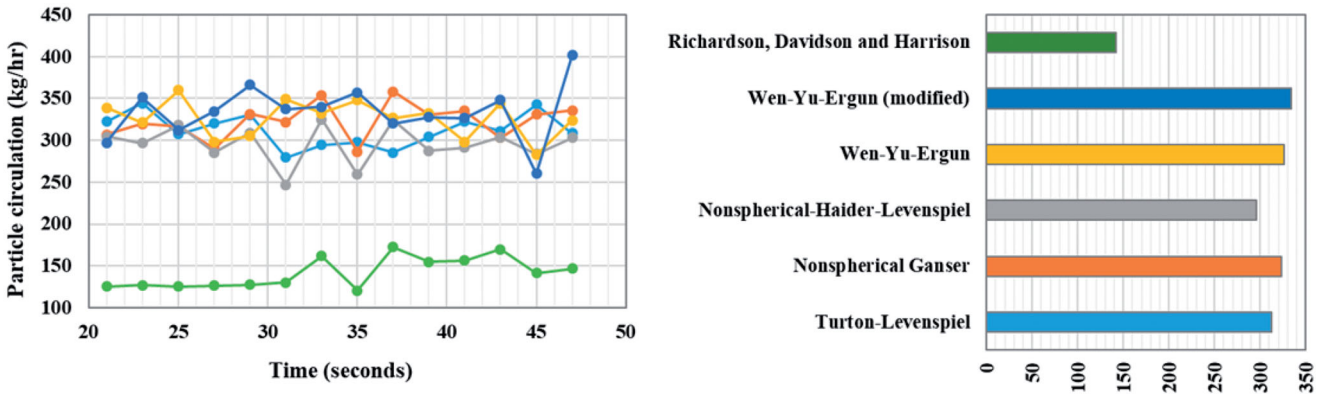

Figure 13. Effect of the drag model for particle circulation rate.

nonspherical Haider-Levenspiel model showed 300 kg/hr where all other drag models resulted in increased circulation above 300 kg/hr reaching the experimental data. Particle volume fractions and particle Reynold number (*Re*) are greatly varied over the reactor. High *Re* and low particle volume fractions can be observed in the riser whereas low *Re* and high particle volume fractions in the loop seal section. The Richardson-Davidson-Harrison drag model is not a function of both parameters at high Reynolds number where the particle volume fraction is excluded in the full range of *Re*, which can be the reason for the large deviation. The particle sphericity was taken as 0.9 for models with sphericity as a parameter (Rorato et al. 2019); Nonspherical-Ganser and Nonspherical-Haider-Levenspiel. Both of the models are a function of *Re* in the full range of *Re*, which is not the case for Wen-Yu model as the drag turns into a constant at high *Re*. These differences might lead to varied results for particle circulation. The laminar and turbulent coefficients of the Ergun model have been subjected to continuous modifications depending on particle properties (i.e. Geldart's classification, particle shape, etc.) (Olatunde and Fasina 2019; Ozahi, Gundogdu, and Carpinlioglu 2008). As the coefficients are increased, both bed pressure drop and fluid drag change proportionally, which is clearly illustrative with increased particle circulation with modified coefficients. The system pressure followed the same trend and approximately same results as depicted in Figure 7.

4. Conclusion

The main objective of the research work was to develop a hydrodynamic model for a circulating fluidized bed system using the Barracuda VR CPFD package, which uses the MP-PIC modeling. Effect of the grid resolution and selected simulation parameters were compared with experimental results and the rate of particle circulation was considered as the primary parameter. The system pressure was also monitored.

The grid resolution near the loopseal showed a great influence over the particle circulation rate and grid refinements at the particular section was needed to capture the particle hydrodynamics. Nearly, 40% increment of particle circulation rate was achieved analogous with loopseal grid refinement. Computational Grid 04 and 05 were successful in achieving the particle circulation similar to the experimental data. The system pressure predictions from the simulations were lower than the experimental data, which could be due to associated uncertainties of geometry and particle properties. The number of computational particles defined by the default software settings was observed to be adequate and further increment did not make considerable changes in the circulation rate. The particle circulation rate increased proportionally by 17% as the closed pack volume fraction was changed from 0.56 to 0.6. The effect of the particle-wall interaction coefficient was less significant compared to closed pack volume fraction where approximately 10%

difference was observed from 0.55 to 0.85. Pressure constant in the particle stress model showed the greatest impact on the particle circulation rate with an increment of 57% as the pressure constant changed from 2.5 to 5. The Wen-Yu-Ergun and Nonspherical Ganser drag models resulted in the highest particle circulation rate where Richardson-Davidson-Harrison model under predicted the circulation.

Precise information about the particle properties will be useful in further analysis and concrete validation of the hydrodynamic model. Model validation for different materials with different size and density will improve the reproducibility of the simulation data. If the experimental unit is equipped to measure the particle loading over different sections, it will be useful for further comparison. Whenever the Ergun equation is used, it is a good practice to optimize the linear coefficient experimentally, especially for the particles not grouped within Geldart B. The uncertainties and measurement errors should be minimized to optimize the model parameters. The developed hydrodynamic model is possible to analyze system behaviors against different operational conditions.

Acknowledgement

The authors like to forward their gratitude to University College of Southeast Norway for providing the Barracuda VR CFD package and computer resources for simulation.

References

Abbasi, A., P. E. Ege, and H. I. de Lasa. 2011. CPFD simulation of a fast fluidized bed steam coal gasifier feeding section. *Chemical Engineering Journal* 174 (1):341–50. doi: 10.1016/j.cej.2011.07.085.

Andrews, M. J., and P. J. O'Rourke. 1996. The multiphase particle-in-cell (MP-PIC) method for dense particulate flows. *International Journal of Multiphase Flow* 22 (2):379–402. doi: 10.1016/0301-9322(95)00072-0.

Basu, P., and J. Butler. 2009. Studies on the operation of loop-seal in circulating fluidized bed boilers. *Applied Energy* 86 (9):1723–31. doi: 10.1016/j.apenergy.2008.11.024.

Chen, C., J. Werther, S. Heinrich, H.-Y. Qi, and E.-U. Hartge. 2013. CPFD simulation of circulating fluidized bed risers. *Powder Technology* 235:238–47. doi: 10.1016/j.powtec.2012.10.014.

Chhabra, R. P., L. Agarwal, and N. K. Sinha. 1999. Drag on non-spherical particles: An evaluation of available methods. *Powder Technology* 101 (3):288–95. doi: 10.1016/S0032-5910(98)00178-8.

Chiesa, M., V. Mathiesen, J. A. Melheim, and B. Halvorsen. 2005. Numerical simulation of particulate flow by the Eulerian–Lagrangian and the Eulerian–Eulerian approach with application to a fluidized bed. *Computers and Chemical Engineering* 29 (2):291–304. doi: 10.1016/j.compchemeng.2004.09.002.

Cui, H., and J. R. Grace. 2007. Fluidization of biomass particles: A review of experimental multiphase flow aspects. *Chemical Engineering Science* 62 (1–2):45–55. doi: 10.1016/j.ces.2006.08.006.

Deen, N. G., M. Van Sint Annaland, M. A. Van der Hoef, and J. A. M. Kuipers. 2007. Review of discrete particle modeling of fluidized beds. *Chemical Engineering Science* 62 (1–2):28–44. doi: 10.1016/j.ces.2006.08.014.

Ergun, S. 1952. Fluid flow through packed columns. *Chemical Engineering Progress* 48:89–94.

Jayarathna, C. K., M. Balfe, B. M. E. Moldestad, and L.-A. Tokheim. 2019. Improved multi-stage cross-flow fluidized bed classifier. *Powder Technology* 342:621–9. doi: 10.1016/j.powtec.2018.10.026.

Jiang, Y., G. Qiu, and H. Wang. 2014. Modelling and experimental investigation of the full-loop gas–solid flow in a circulating fluidized bed with six cyclone separators. *Chemical Engineering Science* 109: 85–97. doi: 10.1016/j.ces.2014.01.029.

Klenov, O. P., A. S. Noskov, and O. A. Parahin. 2017. Investigation of behaviors of the circulating fluidized bed. *Chemical Engineering Journal* 329:66–76. doi: 10.1016/j.cej.2017.06.092.

Li, J., and M. Kwauk. 2003. Exploring complex systems in chemical engineering—the multi-scale methodology. *Chemical Engineering Science* 58 (3–6):521–35. doi: 10.1016/S0009-2509(02)00577-8.

Li, T., A. Gel, S. Pannala, M. Shahnam, and M. Syamlal. 2014. CFD simulations of circulating fluidized bed risers, part I: Grid study. *Powder Technology* 254:170–80. doi: 10.1016/j.powtec.2014.01.021.

Li, X. T., J. R. Grace, C. J. Lim, A. P. Watkinson, H. P. Chen, and J. R. Kim. 2004. Biomass gasification in a circulating fluidized bed. *Biomass and Bioenergy* 26 (2):171–93. doi: 10.1016/S0961-9534(03)00084-9.

Liang, Y., Y. Zhang, T. Li, and C. Lu. 2014. A critical validation study on CPFD model in simulating gas–solid bubbling fluidized beds. *Powder Technology* 263:121–34. doi: 10.1016/j.powtec.2014.05.003.

Loha, C., H. Chattopadhyay, and P. K. Chatterjee. 2014. Three dimensional kinetic modeling of fluidized bed biomass gasification. *Chemical Engineering Science* 109:53–64. doi: 10.1016/j.ces.2014.01.017.

Ma, H., and Y. Zhao. 2018. Investigating the fluidization of disk-like particles in a fluidized bed using CFD-DEM simulation. *Advanced Powder Technology* 29 (10):2380–93. doi: 10.1016/j.apt.2018.06.017.

Moliner, C., F. Marchelli, N. Spanachi, A. Martinez-Felipe, B. Bosio, and E. Arato. 2018. CFD simulation of a spouted bed: Comparison between the Discrete Element Method (DEM) and the Two Fluid Model (TFM). *Chemical Engineering Journal* 377:120446. doi: 10.1016/j.cej.2018.11.164.

O'Rourke, P. J., and D. M. Snider. 2014. A new blended acceleration model for the particle contact forces induced by an interstitial fluid in dense particle/fluid flows. *Powder Technology* 256:39–51. doi: 10.1016/j.powtec.2014.01.084.

Olatunde, G., and O. Fasina. 2019. Modified Ergun equation for airflow through packed bed of loblolly pine grinds. *KONA Powder and Particle Journal Advpub* 36 (0):232. doi: 10.14356/kona.2019003.

Ozahi, E., M. Y. Gundogdu, and M. Ö. Carpinlioglu. 2008. A modification on Ergun's correlation for use in cylindrical packed beds with non-spherical particles. *Advanced Powder Technology 19* (4):369–81. doi: 10.1163/156855208X314985.

Pannala, S., M. Syamlal, and T. J. O'Brien. 2011. *Computational gas-solids flows and reacting systems: Theory, methods and practice*. Hershey, USA: Engineering Science Reference.

Patel, M. K., K. Pericleous, and M. Cross. 1993. Numerical modelling of circulating fluidized beds. *International Journal of Computational Fluid Dynamics* 1 (2):161–76. doi: 10.1080/10618569308904470.

Qiu, G., J. Ye, and H. Wang. 2015. Investigation of gas–solids flow characteristics in a circulating fluidized bed with annular combustion chamber by pressure measurements and CPFD simulation. *Chemical Engineering Science* 134:433–47. doi: 10.1016/j.ces.2015.05.036.

Rorato, R., M. Arroyo, E. Andò, and A. Gens. 2019. Sphericity measures of sand grains. *Engineering Geology* 254:43. doi: 10.1016/j.enggeo.2019.04.006.

Snider, D. M. 2001. An Incompressible Three-Dimensional Multiphase Particle-in-Cell Model for Dense Particle Flows. *Journal of Computational Physics* 170 (2):523–49. doi: 10.1006/jcph.2001.6747.

Snider, D. M. 2007. Three fundamental granular flow experiments and CPFD predictions. *Powder Technology* 176 (1):36–46. doi: 10.1016/j.powtec.2007.01.032.

Snider, D. M., and S. Banerjee. 2010. Heterogeneous gas chemistry in the CPFD Eulerian–Lagrangian numerical scheme (ozone decomposition). *Powder Technology* 199 (1):100–6. doi: 10.1016/j.powtec.2009.04.023.

Snider, D. M., S. M. Clark, and P. J. O'Rourke. 2011. Eulerian–Lagrangian method for three-dimensional thermal reacting

flow with application to coal gasifiers. *Chemical Engineering Science* 66 (6):1285–95. doi: 10.1016/j.ces.2010.12.042.

Thapa, R. K., A. Frohner, G. Tondl, C. Pfeifer, and B. M. Halvorsen. 2016. Circulating fluidized bed combustion reactor: Computational particle fluid dynamic model validation and gas feed position optimization. *Computers and Chemical Engineering* 92:180–8. doi: 10.1016/j.compchemeng.2016.05.008.

Tricomi, L., T. Melchiori, D. Chiaramonti, M. Boulet, and J. M. Lavoie. 2017. Sensitivity analysis and accuracy of a CFD-TFM approach to bubbling bed using pressure drop fluctuations. *Frontiers in Bioengineering and Biotechnology* 5 (38): doi: 10.3389/fbioe.2017.00038.

Tu, Q., and H. Wang. 2018. CPFD study of a full-loop three-dimensional pilot-scale circulating fluidized bed based on EMMS drag model. *Powder Technology* 323:534–47. doi: 10.1016/j.powtec.2017.09.045.

Turton, R., and O. Levenspiel. 1986. A short note on the drag correlation for spheres. *Powder Technology* 47 (1):83–6. doi: 10.1016/0032-5910(86)80012-2.

Wang, Q., H. Yang, P. Wang, J. Lu, Q. Liu, H. Zhang, L. Wei, and M. Zhang. 2014a. Application of CPFD method in the simulation of a circulating fluidized bed with a loop seal Part II—Investigation of solids circulation. *Powder Technology* 253:822–8. doi: 10.1016/j.powtec.2013.11.040.

Wang, Q., H. Yang, P. Wang, J. Lu, Q. Liu, H. Zhang, L. Wei, and M. Zhang. 2014b. Application of CPFD method in the simulation of a circulating fluidized bed with a loop seal, part I—Determination of modeling parameters. *Powder Technology* 253:814–21. doi: 10.1016/j.powtec.2013.11.041.

Wang, W., B. Lu, N. Zhang, Z. Shi, and J. Li. 2010. A review of multiscale CFD for gas–solid CFB modeling. *International Journal of Multiphase Flow* 36 (2):109–18. doi: 10.1016/j.ijmultiphaseflow.2009.01.008.

Xie, J., W. Zhong, B. Jin, Y. Shao, and H. Liu. 2012. Simulation on gasification of forestry residues in fluidized beds by Eulerian–Lagrangian approach. *Bioresource Technology* 121:36–46. doi: 10.1016/j.biortech.2012.06.080.